Monthly Notices
of the
ROYAL ASTRONOMICAL SOCIETY

MNRAS **442,** 2620–2636 (2014) doi:10.1093/mnras/stu964

Magnetic activity and orbital periods of five low-mass eclipsing binaries

Li-Yun Zhang,[1,2]★ Qing-feng Pi[1,2] and Yuan-Gui Yang[3]

[1]*Department of Physics, College of Science, Guizhou University and NAOC-GZU-Sponsored Center for Astronomy, Guizhou University, Guiyang 550025, People's Republic of China*
[2]*Key Laboratory for the Structure and Evolution of Celestial Objects, Chinese Academy of Sciences, Kunming 650011, People's Republic of China*
[3]*School of Physics and Electronic Information, Huaibei Normal University, Huaibei 235000, Anhui Province, People's Republic of China*

Accepted 2014 May 12. Received 2014 May 12; in original form 2014 January 30

ABSTRACT

We report 15 new *VRI* light curves of five low-mass eclipsing binaries (NSVS 02502726, NSVS 07453183, NSVS 11868841, NSVS 06550671 and NSVS 10653195) that were observed between 2010 and 2012. We analysed our new data together with three published spectroscopic observations and seven published light curves using a modified version of the Wilson–Devinney program. Orbital solutions of the five low-mass eclipsing binaries were revised and new star-spot parameters were obtained. We found that spot locations on the five low-mass eclipsing binaries changed over several years. However, the star-spots for NSVS 07453183 and NSVS 06550671 were stable for several months. More interestingly, for NSVS 02502726, the spots within a star-spot longitude region of 180°–360° indicated a magnetic activity cycle of 5.9(±0.2) yr. Moreover, we detected the first flare-like event on NSVS 07453183 at phase 0.39. The observations of the chromospheric activity indicators (Hβ and Hγ lines) revealed that NSVS 10653195 and NSVS 06550671 were active. For NSVS 02502726, we found a weak continuous secular decrease at a smaller rate of $dp/dt = -2.1(0.8) \times 10^{-7}$ d yr^{-1} than the previous result. For NSVS 07453183, the O−C times appeared to increase at cycle 6000, and this was followed by a decrease at cycle 6500.

Key words: binaries: eclipsing – stars: individual: NSVS 02502726 – stars: individual: NSVS 06550671 – stars: individual: NSVS 11868841 – stars: individual: NSVS 07453183 – stars: individual: NSVS 10653195.

1 INTRODUCTION

Rapidly rotating low-mass stars (M star $< 0.8\,m_{\odot}$) exhibit phenomena associated with magnetic activity, such as evidence of star-spots, plage and flares (e.g. Güdel 2002; Pribulla, Chochol & Vittone 2003; Berdyugina 2005; Hall 2008; Strassmeier 2009; Lanza 2010). However, in many such kinds of stars, details of the active phenomena are not well understood. In order to have a better understanding of the stellar magnetic activity, we need to monitor the late-type stars by multicolour photometry, and medium and high-resolution spectroscopy.

Although low-mass stars, which we define as having $M < 0.8\,m_{\odot}$, are the most populous stellar objects in the Galaxy (e.g. Henry, Kirkpatrick & Simons 1994; Chabrier 2003; Reid et al. 2004; Ribas 2006a, 2007; Nefs et al. 2012), until now, only about 30 low-mass eclipsing binaries (including M dwarfs that orbit higher mass stars) with determined masses, radii, luminosities and temperatures have been detected (e.g. Morales, Ribas & Jordi 2008; Ribas et al. 2008; Çakirli, Ibanoğlu & Güngör 2009; Çakirli, Ibanoğlu & Sipahi 2013). The reason there are so few low-mass eclipsing binaries is that they have to be aligned to eclipse and they have low intrinsic brightness (Torres & Ribas 2002; Blake et al. 2008; Irwin et al. 2009; Morales et al. 2009). However, even in such small numbers, a detailed comparison of observed masses and radii with theoretical predictions has revealed large disagreements (e.g. López-Morales & Ribas 2005). Current evolutionary models predict radii of stars in the 0.4–$0.8\,m_{\odot}$ range to be 5–15 per cent smaller than observed radii and a 3–5 per cent larger effective temperature than the observed temperature (e.g. Baraffe et al. 1998; Ribas 2006a,b; Ribas et al. 2008; Coughlin et al. 2011). Several authors have discussed possible scenarios of these discrepancies between models and observations of low-mass stars (e.g. Baraffe et al. 1998; Torres & Ribas 2002; López-Morales & Ribas 2005; Ribas et al. 2008; Morales et al. 2010). These include magnetic activity (López-Morales 2007; Morales et al. 2008, 2010), fast rotation (Chabrier, Gzllardo & Baraffe 2007), metallicity (López-Morales 2007) or their combined action. The magnetic activity of low-mass eclipsing binaries is an important aspect of the discrepancies. Moreover, studying the magnetic activity of low-mass stars provides an opportunity and key constraint for stellar and solar dynamo

★E-mail: liy_zhang@hotmail.com

Table 1. All published photometric and spectroscopic solutions of the five eclipsing binaries.

Star (NSVS)	Rotation period (d)	Method	$q_{ph}(M2/M1)$	$q_{sp}(M2/M1)$	$M1(M\odot)$	$M2(M\odot)$	$R1(R\odot)$	$R2(R\odot)$	$i(^\circ)$	$T1$(k)	$T2$(k)	Ω_1	Ω_2	Reference
02502726	0.559 755	Light+radial	–	0.486	0.714	0.347	0.674	0.763	87	4300	3620	4.8	3.862	1
02502726	0.559 778	Light+radial	–	0.496	0.689	0.341	0.707	0.657	88	4298	3843	4.57	3.42	2
02502726	0.559 772	Light	0.83	–	0.690	0.570	0.830	0.750	88.2	4370	3950	–	–	3
07453183	0.366 971	Light	0.93	–	0.730	0.680	0.790	0.720	89.1	3570	3340	–	–	3
11868841	0.601 790	Light	0.93	–	0.940	0.87	1.03	0.93	87.5	3970	3750	–	–	3
11868841	0.601 790	Light+radial	–	0.698	0.870	0.607	0.983	0.901	88	5250	5020	4.262	3.79	4
06550671	0.192 637	Light+radial	–	0.51	0.51	0.26	0.55	0.29	72.5	3735	3106	2.944	3.545	5
10653195	0.560 721	Light	0.91	–	0.67	0.61	0.79	0.67	85.4	4120	3920	–	–	3
10653195	0.560 723	Light	–	–	0.67	0.61	0.71	0.67	85.7	3920	3825	–	–	6

q_{ph} represents the result from photometric study. q_{sp} represents the result from spectroscopic study.
References – 1. Çakirli et al. (2009), 2. Lee et al. (2013), 3. Coughlin & Shaw (2007), 4. Çakirli, Ibanoğlu & Dervisoglu (2010), 5. Dimitrov & Kjurkchieva (2010), 6. Wolf et al. (2010).

Table 2. The observational log.

Star name	Spectral type	Comparison	Check star	Exposure time	Number(*VRI*)
NSVS 02502726	M dwarf	GSC 3798−1250	GSC 3798−1234	120 s, 60 s, 40 s	1099, 1089, 1089
NSVS 07453183	M2*	TYC 2499−356-1	Star (09:15:47.04; 36:13:54.7)	60 s, 40 s, 30 s	574, 574, 574
NSVS 11868841	G9±2+	Star (23:17:32.4; 19:21:28.7)	Star (23:18:03; 19:12:47.3)	120 s, 60 s, 60 s	348, 346, 345
NSVS 06550671	M dwarf	TYC 2314−780-1	Star (02:20:34.15; 33:21:07.7)	90 s, 40 s, 10 s	453, 452, 453
NSVS 10653195	k7*	Star (16:07:14.6; 12:15:53.6)	Star (16:07:47.4; 12:16:32.8)	120 s, 90 s, 60 s	262, 258, 258

Notes. For some comparison and check stars, we only give their RA and Dec. Spectral type (which was marked by *) was assumed using the colour index (Cox 2000).

theory (Berdyugina 2005; Strassmeier 2009). Therefore, it is necessary to monitor the magnetic activity of low-mass eclipsing binaries.

The five eclipsing binaries in this study (NSVS 02502726, NSVS 07453183, NSVS 11868841, NSVS 06550671 and NSVS 10653195) were discovered to be variable stars from the Northern Sky Variability Survey (NSVS; Woźniak et al. 2004). They show considerable distortions out of eclipse (e.g. Coughlin & Shaw 2007; Çakirli et al. 2009; Çakirli et al. 2010; Dimitrov & Kjurkchieva 2010; Wolf et al. 2010; Pribulla et al. 2012; Lee et al. 2013) and two of them (NSVS 02502726 and NSVS 06550671) show Hα emission (Çakirli et al. 2009, 2010). NSVS 06550671 (GSC 2314−0530, 1RXS J022050.7+332049) was an interesting eclipsing binary (Norton et al. 2007; Dimitrov & Kjurkchieva 2010) that was also assigned as SWASP J022050.85+332047.6 according to the SuperWasp photometric survey (Pollacco et al. 2006). Furthermore, Dimitrov & Kjurkchieva (2010) obtained multicolour CCD *VRI* photometric and spectroscopic observations of NSVS 06550671, and determined their global eclipse parameters. As for NSVS 02502726, NSVS 07453183, NSVS 11868841 and NSVS 10653195, Coughlin & Shaw (2007) obtained the orbital and star-spot parameters using an Eclipsing Light Curve programme (Orosz & Hauschildt 2000). Recently, Çakirli et al. (2010) presented an optical spectroscopy and an extensive *R*- and *I*-band photometry, and derived the principal parameters of NSVS 02502726, especially stellar mass and radius, by simultaneously analysing the light and radial velocities curves. Çakirli et al. (2009) derived the orbital parameters of NSVS 11868841 by analysing the radial velocity curves and the existing *VRI* bandpass light curves (LCs). All the published photometric and spectroscopic solutions of the five low-mass eclipsing binaries are summarized in Table 1. Until now, there has been no period variation analysis of NSVS 07453183, NSVS 11868841, NSVS 06550671 and NSVS 10653195, and only one study of NSVS 02502726, where an orbital period analysis revealed that the period has experienced a continuous decrease of -5.9×10^{-7} d yr^{-1} with a weak sinusoidal variation (Lee et al. 2013).

2 OBSERVATIONS

In this paper, we carried out new photometric observations of the five low-mass eclipsing binaries from 2010 to 2012 (NSVS 02502726: 2010 November 26, 27, 28 and 29; 2011 January 29 and 31, and December 10, 11, and 13; 2012 February 18 and 20, and April 3, 6, 7 and 8; NSVS 07453183: 2011 March 22, 24, April 15, 17, and 18, and December 8, 9; NSVS 11868841: 2010 November 26, 27, 28, 29, and December 11, 12, 13, 15; GSC02314−00530: 2010 November 24; 2011 January 28, and February 1, and December 9; NSVS 10653195: 2012 April 3, 4, 6, 7, and 8) with an 85 cm telescope at Xinglong station of National Astronomical Observatories of China (NAOC). The photometer was equipped with a 1024 × 1024 pixel CCD along with Johnson–Cousins *B*, *V*, *R*, *I* filters (Zhou et al. 2009). Our observations were carried out in *V*, *R* and *I* passbands. We reduced all the observed CCD images by means of the APPHOT sub-package of the Image Reduction and Analysis Facility (IRAF) in the standard fashion (including image trimming, bias subtraction, flat-field division and cosmic ray removal). Our observation log is shown in Table 2, which includes our object names, comparison stars (which were chosen near the target), check stars, typical exposure times and the total number of observations in *VRI* bands. The different magnitudes of our objects and comparison stars (in the sense of our objects minus the comparison stars) were used to construct the LCs and the results are shown in Fig. 1. Since the fields of our objects were not crowded, the technique of aperture photometry was applied to extract the magnitudes. The criterion for choosing the comparison and check stars was that there was no variability in the previous observations (Çakirli et al. 2009; Lee et al. 2013). We also observed no intrinsic variability of the comparison and check

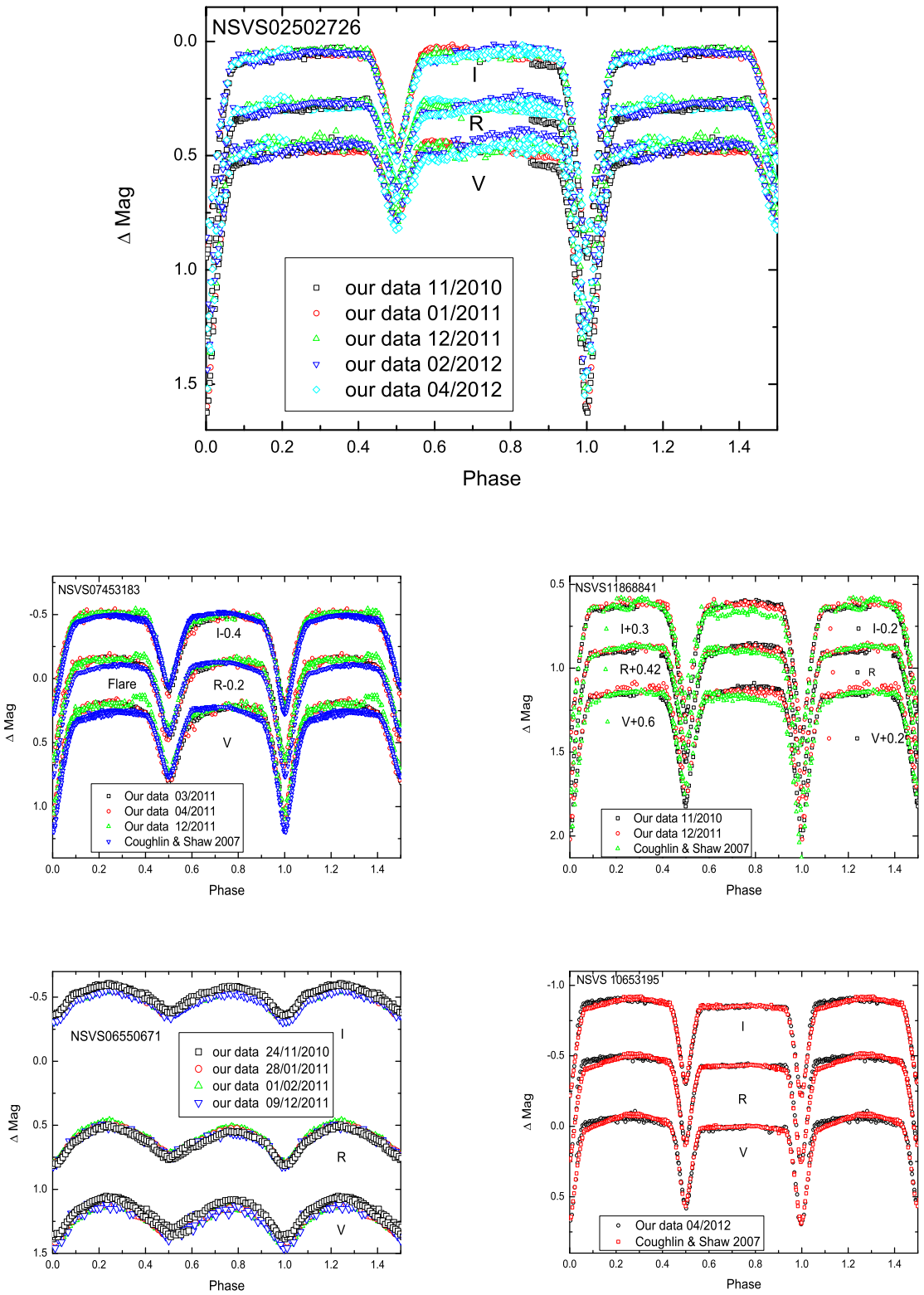

Figure 1. *V*, *R* and *I* LCs of the five low-mass eclipsing binaries. Different kinds of symbols represent the data observed for the different times.

stars. The check star was used to make sure that the comparison star was not itself variable. For NSVS 02502726, our comparison and check stars are the same to those of Çakirli et al. (2009) and Lee et al. (2013). All individual observations are shown in Table 3 in the form of the heliocentric Julian dates (HJD) and the *VRI* differential magnitudes between the eclipsing star and the comparison star (Δ Mag). We note that the scatters of individual points are better than 0.01 mag in all bands.

Table 3. *VRI* observations data of the five low-mass eclipsing binaries collected 2010–2012. (This table is available as online material.)

Star name	HJD_V	Δ Mag_V	HJD_R	Δ Mag _R	HJD_I	Δ Mag_I
NSVS 02502726	2455527.1017	0.497	2455527.1028	0.285	2455527.1034	0.071
NSVS 02502726	2455527.1043	0.487	2455527.1053	0.301	2455527.1060	0.054
.....	.....	.....	.....	.....	.....	.....
NSVS 02502726	2455530.4159	0.514	2455530.4221	0.322	2455530.4202	0.086
NSVS 02502726	2455530.4185	0.506	2455530.4246	0.316	2455530.4227	0.079
NSVS 02502726	2455591.0990	0.577	2455591.0998	0.404	2455591.1002	0.191
NSVS 02502726	2455591.1013	0.551	2455591.1025	0.373	2455591.1033	0.161
.....	.....	.....	.....	.....	.....	.....
NSVS 02502726	2455593.4192	0.457	2455593.4198	0.287	2455593.4217	0.043
NSVS 02502726	2455593.4208	0.461	2455593.4214	0.270		
NSVS 02502726	2456020.9824	0.800	2456020.9833	0.694	2456020.9839	0.507
NSVS 02502726	2456020.9861	0.825	2456020.9871	0.673	2456020.9876	0.523
.....	.....	.....	.....	.....	.....	.....
NSVS 02502726	2456026.1862	0.487				
NSVS 02502726	2456026.1913	0.450				
NSVS 07453183	2455642.9940	0.195	2455642.9948	0.045	2455642.9953	−0.112
NSVS 07453183	2455642.9959	0.204	2455642.9966	0.052	2455642.9971	−0.085
.....	.....	.....	.....	.....	.....	.....
NSVS 07453183	2455645.2193	0.236	2455645.2203	0.082	2455645.2210	−0.083
NSVS 07453183	2455645.2220	0.230	2455645.2230	0.089	2455645.2238	−0.080
NSVS 07453183	2455666.9902	0.260	2455666.9911	0.090	2455666.9918	−0.061
NSVS 07453183	2455666.9926	0.280	2455666.9936	0.120	2455666.9942	−0.085
.....	.....	.....	.....	.....	.....	.....
NSVS 07453183	2455670.1645	0.181	2455670.1653	0.034	2455670.1658	−0.111
NSVS 07453183	2455670.1665	0.294	2455670.1673	0.066	2455670.1678	−0.107
NSVS 07453183	2455904.1525	0.735	2455904.1532	0.574	2455904.1538	0.381
NSVS 07453183	2455904.1544	0.834	2455904.1550	0.593	2455904.1556	0.439
.....	.....	.....	.....	.....	.....	.....
NSVS 07453183	2455905.3112	0.239	2455905.3120	0.070	2455905.3125	−0.070
NSVS 07453183	2455905.3132	0.253	2455905.3140	0.114	2455905.3145	−0.123
NSVS 11868841	2455527.0359	1.032	2455527.0369	0.994	2455527.0378	0.932
NSVS 11868841	2455527.0388	1.046	2455527.0399	0.995	2455527.0407	0.942
.....	.....	.....	.....	.....	.....	.....
NSVS 11868841	2455530.1380	1.003	2455530.1393	0.934	2455530.1404	0.872
NSVS 11868841	2455530.1416	0.976	2455530.1430	0.907	2455530.1440	0.855
NSVS 11868841	2455906.9152	0.936	2455906.9166	0.884	2455906.9175	0.806
NSVS 11868841	2455906.9186	0.945	2455906.9199	0.892	2455906.9209	0.808
.....	.....	.....	.....	.....	.....	.....
NSVS 11868841	2455911.1052	0.933				
NSVS 11868841	2455911.1105	0.956				
NSVS 06550671	2455524.9297	1.283	2455524.9306	0.713	2455524.9311	−0.423
NSVS 06550671	2455524.9318	1.305	2455524.9327	0.753	2455524.9332	−0.401
.....	.....	.....	.....	.....	.....	.....
NSVS 06550671	2455525.2456	1.323	2455525.2486	0.632	2455525.2470	−0.463
NSVS 06550671					2455525.2491	−0.471
.....	.....	.....	.....	.....	.....	.....
NSVS 10653195	2456021.2032	−0.011	2456021.2048	−0.471	2456021.2061	−0.876
NSVS 10653195	2456021.2080	−0.029	2456021.2097	−0.476	2456021.2108	−0.876
.....	.....	.....	.....	.....	.....	.....
NSVS 10653195	2456026.3738	−0.065				
NSVS 10653195	2456026.3773	−0.026				

Since no spectroscopic studies on Hβ and Hγ lines of NSVS 10653195 and NSVS 06550671 have been reported, we carried out a systematic analysis of spectroscopic observations in the literature to understand chromospheric activity. Our spectroscopic observations of NSVS 06550671 and NSVS 10653195 (Fig. 2) were carried out with an optical median resolution (OMR) spectrograph of a 2.16 m telescope at the Xinglong station of the NAOC in 2012. The OMR spectrograph was centred at about 4280 Å with a reciprocal dispersion of 1.03 Å pixel^{-1} and a wavelength range of 3700–4960 Å (Fang et al. 2010). The observational exposure time of NSVS 06550671 and NSVS 10653195 were 20 and 30 min, respectively. We also obtained high S/N spectra of inactive

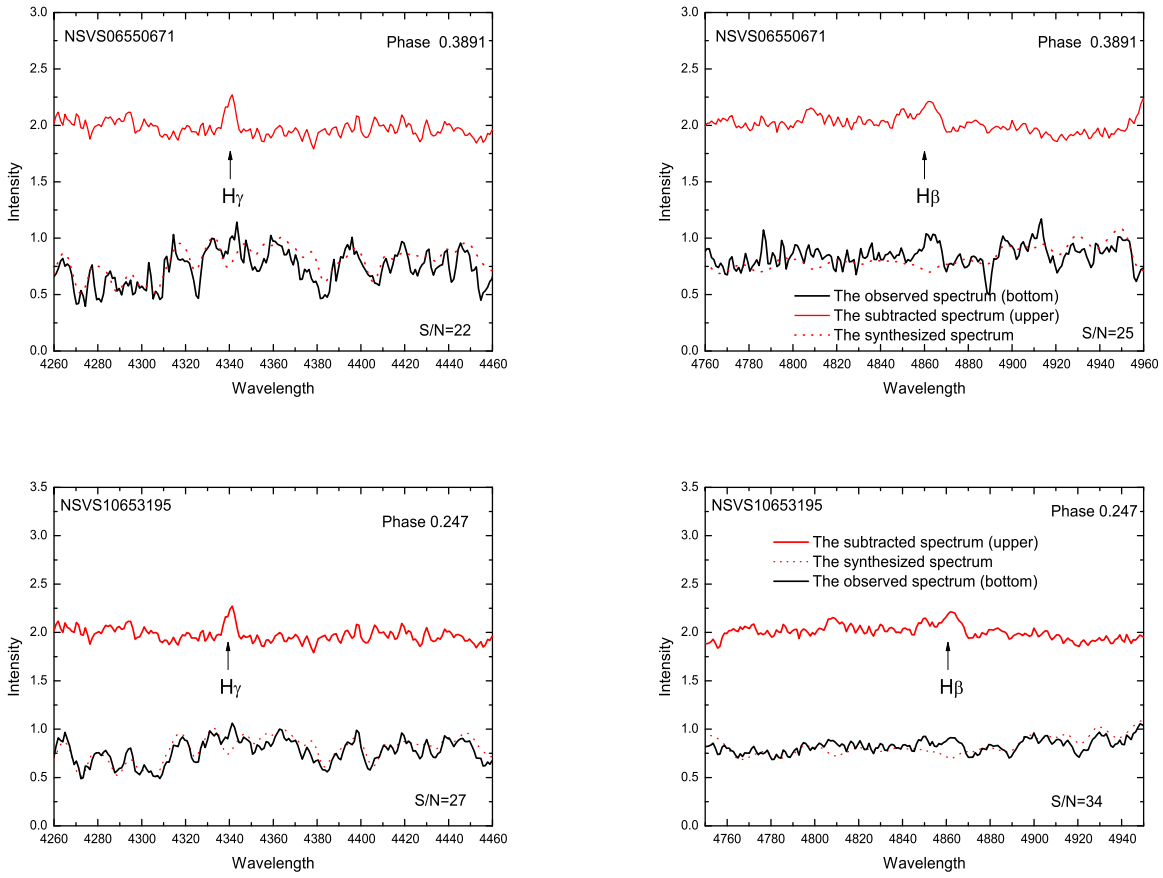

Figure 2. Samples of the observed, synthesized and subtracted spectra including the Hβ and Hγ lines of NSVS 06550671 and NSVS 10653195. The dotted lines represent the synthesized spectra and the upper spectra correspond to the subtracted spectra.

stars HR 2458 (M1 dwarf) and HR 2216 (M3 dwarf) that were used as templates. We performed a reduction of the spectra using IRAF packages, which involved bias subtraction, flat-fielding, cosmic ray removal, one-dimensional spectrum extraction and wavelength calibration.

3 PERIOD AND EPOCH DETERMINATION

Based on our new observations, we separately determined new times of light minima for all three bands using the previously used program (Kwee & van Woerden 1956; Nelson 2007). The corresponding errors were determined by the covariance matrix of the least-squares fit, which underestimates the uncertainties because it does not account for systematic errors. For the minima, each colour is individually fitted, and the eclipsing minimum times with their errors and observational filters are listed in Table 4. The results combined for each epoch are also listed in Table 4. To calculate an updated ephemeris and period variation, all available eclipse times were collected from the literature and included in the analysis (Table 5). Using these minimum times, an updated linear ephemeris was then obtained for each system by using a least-squares fit, as listed in Table 6. All minima were weighted equally because there were no published errors of the 10 minima, and they were all observed with a similar CCD method. Based on our new ephemeris, the O−C values of minimum times are calculated and listed in Table 5. To clarify the period change, we plotted these values in Fig. 3. It seems that there may be a weak variation of NSVS 02502726 when using the reduced chi-square test. The least-squares method was then used to obtain the following quadratic ephemeris.

NSVS 02502726 :

$$\mathrm{Min.}I = \mathrm{JD(Hel.)}2454497.5500(\pm0.0001) + 0.559\,7788(\pm0.000\,000\,01)E - 1.6(\pm0.6)\times10^{-10}\times E^2\,\mathrm{d}. \quad (1)$$

This suggests a weak continuous secular decrease of the period at a rate of $\mathrm{d}p/\mathrm{d}t = -2.1(0.8)\times10^{-7}\,\mathrm{d\,yr^{-1}}$ for NSVS 02502726. For NSVS 07453183, the O–C times appear to increase at cycle 6000, then decrease at cycle 6500. For NSVS 11868841, NSVS 6550671 and NSVS 10653195, but there are no obvious variations.

4 LC ANALYSIS

We plotted the LCs of our new observations in Fig. 1, where the phases of data points were calculated using the newly derived epochs. The new observations allowed us to analyse orbital and star-spot parameters, and chromospheric activity.

4.1 The orbital parameters and star-spot parameters

We detected out-of-eclipse distortions in the LCs for our objects, as shown in Fig. 1. Since our data have a high time resolution

Table 4. New minimum times of the five low-mass eclipsing binaries.

Star name	*V*		*R*		*I*		Mean (*VRI*)		Min
NSVS	HJD 245,+	Error	HJD 245,+	Error	HJD 245,+	Error	HJD 245,+	Error	1/2
02502726	5529.2216	0.0001	5529.2215	0.0001	5529.2216	0.0001	5529.2216	0.0001	1
02502726	5530.3410	0.0001	5530.3410	0.0001	5530.3410	0.0001	5530.3410	0.0001	1
02502726	5591.3568	0.0001	5591.3567	0.0001	5591.3568	0.0001	5591.3568	0.0001	1
02502726	5593.3156	0.0001	5593.3158	0.0001	5593.3159	0.0001	5593.3158	0.0001	2
02502726	5906.2337	0.0007	5906.2324	0.0004	5906.2323	0.0005	5906.2328	0.0005	2
02502726	5907.3516	0.0005	5907.3512	0.0004	5907.3514	0.0005	5907.3514	0.0005	2
02502726	5909.3108	0.0003	5909.3112	0.0001	5909.3111	0.0001	5909.3110	0.0002	1
02502726	5976.2052	0.0004	5976.2048	0.0003	5976.2048	0.0004	5976.2049	0.0004	2
02502726	5978.1645	0.0009	5978.1645	0.0009	5978.1645	0.0003	5978.1645	0.0008	1
02502726	6024.0656	0.0004	6024.0656	0.0002	6024.0655	0.0002	6024.0656	0.0003	1
02502726	6026.0255	0.0003	6026.0254	0.0005			6026.0255	0.0004	1
07453183	5643.0709	0.0006	5643.0709	0.0005	5643.0710	0.0004	5643.0709	0.0005	2
07453183	5645.0885	0.0004	5645.0884	0.0006	5645.0884	0.0003	5645.0884	0.0004	1
07453183	5667.1066	0.0008	5667.1061	0.0004	5667.1068	0.0003	5667.1065	0.0005	1
07453183	5669.1256	0.0006	5669.1249	0.0008	5669.1255	0.0006	5669.1253	0.0007	2
07453183	5670.0419	0.0005	5670.0415	0.0005	5670.0417	0.0004	5670.0417	0.0005	1
07453183	5904.1643	0.0006	5904.1644	0.0004	5904.1645	0.0002	5904.1644	0.0004	1
07453183	5904.3495	0.0006	5904.3488	0.0002	5904.3485	0.0004	5904.3489	0.0004	2
07453183	5905.2654	0.0007	5905.2654	0.0006	5905.2658	0.0006	5905.2655	0.0006	1
11868841	5527.9842	0.0002	5527.9841	0.0001	5527.9679	0.0002	5527.9840	0.0002	1
11868841	5530.0896	0.0001	5530.0896	0.0002	5530.0897	0.0003	5530.0896	0.0002	2
11868841			5907.1136	0.0010	5907.1133	0.0009	5907.1135	0.001	1
11868841	5910.0220	0.0005	5910.0256	0.0005	5910.0253	0.0070	5910.0247	0.0020	2
06550671			5525.0384	0.0004	5525.0379	0.0008	5525.0383	0.0006	2
06500671	5525.1326	0.0001	5525.1332	0.0001	5525.1325	0.0007	5525.1327	0.0003	1
06500671			5525.2297	0.0002	5525.2319	0.0005	5525.2308	0.0003	2
06500671	5594.0027	0.0005	5594.0022	0.0004	5594.0017	0.0004	5594.0022	0.0004	2
06500671	5594.0964	0.0001	5594.0963	0.0001	5594.0964	0.0002	5594.0964	0.0001	1
06500671	5590.0516	0.0003	5590.0513	0.0001	5590.0506	0.0002	5590.0512	0.0002	1
06500671			5589.9567	0.0001	5589.9559	0.0005	5589.9563	0.0003	2
06500671	5905.0101	0.0004	5905.0107	0.0015	5905.0110	0.0023	5905.0106	0.0013	1
06500671			5905.1104	0.0006	5905.1084	0.0005	5905.1094	0.0006	2
10653195	6022.2679	0.0005	6022.2679	0.0005	6022.2680	0.0005	6022.2679	0.0005	1
10653195	6024.2315	0.0004	6024.2314	0.0004	6024.2314	0.0007	6024.2314	0.0005	2
10653195	6025.2315	0.0004	6025.2314	0.0004	6025.2314	0.0007	6025.3528	0.0004	2

Notes. 1 represents the primary minima, and 2 represents the secondary minima.

Table 5. All compiled light minimum times of the low-mass eclipsing binaries. This Table is available as online material.

Star name	JD(Hel.)	Error	Method	Cycle	(O–C)	Residual	Reference
NSVS 02502726	2453692.0274	0.000 12	CCD	−1439.0	−0.0012	−0.0006	2
NSVS 02502726	2453692.8684	0.000 13	CCD	−1437.5	0.0001	0.0007	2
NSVS 02502726	2453728.9730	0.000 13	CCD	−1373.0	−0.0010	−0.0005	2
NSVS 02502726	2454497.2696		CCD	−.5	−0.0004	−0.0005	1
NSVS 02502726	2454497.5502		CCD	.0	0.0004	0.0002	1
NSVS 02502726	2454498.3894		CCD	1.5	−0.0001	−0.0003	1
NSVS 02502726	2454498.6701		CCD	2.0	0.0007	0.0005	1
NSVS 02502726	2454499.2300		CCD	3.0	0.0008	0.0006	1
NSVS 02502726	2454499.5085		CCD	3.5	−0.0006	−0.0007	1
NSVS 02502726	2454500.6284		CCD	5.5	−0.0002	−0.0004	1
NSVS 02502726	2454501.4690		CCD	7.0	0.0007	0.0005	1
NSVS 02502726	2455529.2216	0.0001	CCD	1843.0	−0.0001	−0.0002	4
NSVS 02502726	2455530.3410	0.0001	CCD	1845.0	−0.0002	−0.0003	4
NSVS 02502726	2455591.3568	0.0001	CCD	1954.0	−0.0002	−0.0003	4
NSVS 02502726	2455593.3158	0.0001	CCD	1957.5	−0.0005	−0.0006	4
.....	.....	.....	.....	.....	.....	.....	
NSVS 6550671	2455525.2308	0.0003	CCD	21 663.5	0.0001	0.0007	4
NSVS 6550671	2455589.9563	0.0004	CCD	21 999.5	−0.0001	0.0003	4
NSVS 6550671	2455590.0512	0.0001	CCD	22 000.0	−0.0015	−0.0011	4

Table 5 – *continued*

Star name	JD(Hel.)	Error	Method	Cycle	(O–C)	Residual	Reference
NSVS 6550671	2455594.0022	0.0002	CCD	22 020.5	0.0005	0.0008	4
NSVS 6550671	2455594.0964	0.0003	CCD	22 021.0	−0.0017	− 0.0013	4
NSVS 6550671	2455905.0106	0.0013	CCD	23 635.0	−0.0019	− 0.0025	4
NSVS 6550671	2455905.1094	0.0006	CCD	23 635.5	0.0006	0.0000	4
NSVS 6550671	2455838.4592	0.0031	CCD	23 289.5	0.0025	0.0020	7
NSVS 6550671	2455839.4206	0.0009	CCD	23 294.5	0.0007	0.0002	7
NSVS 6550671	2455839.5158	0.0018	CCD	23 295.0	−0.0004	− 0.0009	7
NSVS 6550671	2455839.6150	0.0015	CCD	23 295.5	0.0024	0.0020	7
NSVS 10653195	2451338.8354	0.0004	CCD	−3451.5	−0.0026	0.0000	8
NSVS 10653195	2453570.5104	0.0009	CCD	528.5	−0.0018	− 0.0023	9
NSVS 10653195	2454581.4947	0.0002	CCD	2331.5	0.0004	0.0000	3
NSVS 10653195	2454592.4287	0.000 09	CCD	2351.0	0.0004	0.0000	3
NSVS 10653195	2454594.39162	0.000 09	CCD	2354.5	0.0008	0.0003	3
NSVS 10653195	2454600.5593	0.0001	CCD	2365.5	0.0005	0.0000	3
NSVS 10653195	2454601.4003	0.000 08	CCD	2367.0	0.0004	0.0000	3
NSVS 10653195	2454975.4021	0.000 12	CCD	3034.0	0.0005	0.0003	3
NSVS 10653195	2453531.8252	0.000 19	CCD	459.5	0.0028	0.0023	2
NSVS 10653195	2453854.7985	0.0006	CCD	1035.5	0.0002	− 0.0004	2
NSVS 10653195	2453856.7613	0.0003	CCD	1039.0	0.0005	− 0.0001	2
NSVS 10653195	2453863.7696	0.000 03	CCD	1051.5	−0.0003	− 0.0009	2
NSVS 10653195	2453865.7324	0.000 03	CCD	1055.0	−0.0001	− 0.0007	2
NSVS 10653195	2453878.9117	0.000 03	CCD	1078.5	0.0023	0.0017	2
NSVS 10653195	2456022.2679	0.0005	CCD	4901.0	−0.0020	− 0.0007	4
NSVS 10653195	2456024.2314	0.0005	CCD	4904.5	−0.0010	0.0003	4
NSVS 10653195	2456025.3528	0.0004	CCD	4906.5	−0.0010	0.0002	4

Notes. (1) Çakirli et al. (2009), (2) Coughlin & Shaw (2007), (3) Wolf et al. 2010, (4) this paper, (5) Lee et al. (2013), (6) Paschke & Brát (2006), http://var.astro.cz/ocgate/, (7) Banfi et al. 2012, (8) Kazarovets, Samus & Durlevich (1998), (9) ASAS: Pojmański (1998).

Table 6. Calculated periods and epochs.

Star	*T*0(HJD)	Error	Period	Error
NSVS 02502726	2454497.5498	0.0001	0.559 778 50	0.000 000 07
NSVS 07453183	2453456.8600	0.0003	0.366 967 53	0.000 000 08
NSVS 11868841	2453663.0280	0.0004	0.601 7937	0.000 0002
NSVS 06550671	2451352.0618	0.0014	0.192 635 95	0.000 000 07
NSVS 10653195	2453274.1705	0.0005	0.560 7222	0.000 0002

and full phase coverage (except for NSVS 10653195), the orbital solutions of the low-mass eclipsing binaries could be well derived using an updated version of the Wilson–Devinney (WD) program (Wilson & Devinney 1971; Wilson 1990, 1994; Wilson & Van Hamme 2004/2010, related references). For NSVS 02502726, NSVS 11868841 and NSVS 06550671, the radial velocity observations were carried out by Çakirli et al. (2009, 2010) and Dimitrov & Kjurkchieva (2010), respectively. Therefore, our *VRI* LCs and the published radial velocities were analysed simultaneously to obtain the photometric–spectroscopic elements. For NSVS 07453183 and NSVS 10653195, since there have been no previous spectroscopic observations, we have used the relationship of a reliable mass ratio and the weighted sum of squares of residuals to find reasonable results. Although we could not obtain LCs with sufficient phase coverage, we derived the geometric parameters, since there was only a small gap. We used an updated version of the WD program to calculate the orbital solutions of the low-mass eclipsing binaries (Wilson & Devinney 1971; Wilson 1990, 1994; Wilson & Van Hamme 2004/2010), which were implemented using the FORTRAN programming language. The procedure of photometric solution consisted of three consecutive steps (Zhang & Gu 2007): (1) The first step of our procedure was to adjust the orbital parameters that were selected, in order to obtain a theoretical LC without maculation effects using those parts of the observed LC that were least affected by the spots. (2) The second step of our procedure involved adjusting the spot parameters in order to fit the remaining parts of the LCs, especially, to reproduce the shapes of the distortion outside the eclipses. (3) The final step was to separately adjust the orbital parameters and spot parameters again until they converged or the theoretical curves fitted the observed ones well. The details of the procedure for the orbital solution are similar to those in our previous works of several eclipsing binaries of RT And (Zhang & Gu 2007), DV Psc (Zhang, Zhang & Zhu 2010a), GSC 3576−0170 (Zhang et al. 2010b), KQ Gem (Zhang 2010) and V1034 Her (Zhang 2012).

During the process, the gravity-darkening exponents were set at 0.32 according to the stellar temperatures given by Claret (2000). The bolometric albedo $A_1 = A_2 = 0.5$ (Rucinski 1969) were set for late-type stars with a convective envelope. The primary temperatures were taken from the previously assumed results (e.g. Coughlin & Shaw 2007; Çakirli et al. 2009; Dimitrov & Kjurkchieva 2010), which were derived by the infrared colours of the 2MASS catalogue (Skrutskie et al. 1997) with the infrared colour–effective temperature relationship given by Tokunaga (2000). Linear limb-darkening law was used to compute the limb-darkening effect from van Hamme (1993). It should be mentioned here that there have been no spectroscopic observations for NSVS 07453183 and NSVS 10653195. Hence, we explored a wide range (0.2–3.0) to search the reasonable mass ratios. However, because of the LC distortions, we failed to obtain a satisfactory fit to both the quadratures of the LCs with an unspotted modelling. Therefore, we set the weights of part of the data (NSVS 07453183 and NSVS 10653195 with phases between 0.6 and 0.9) to zero, and fitted the other part of the

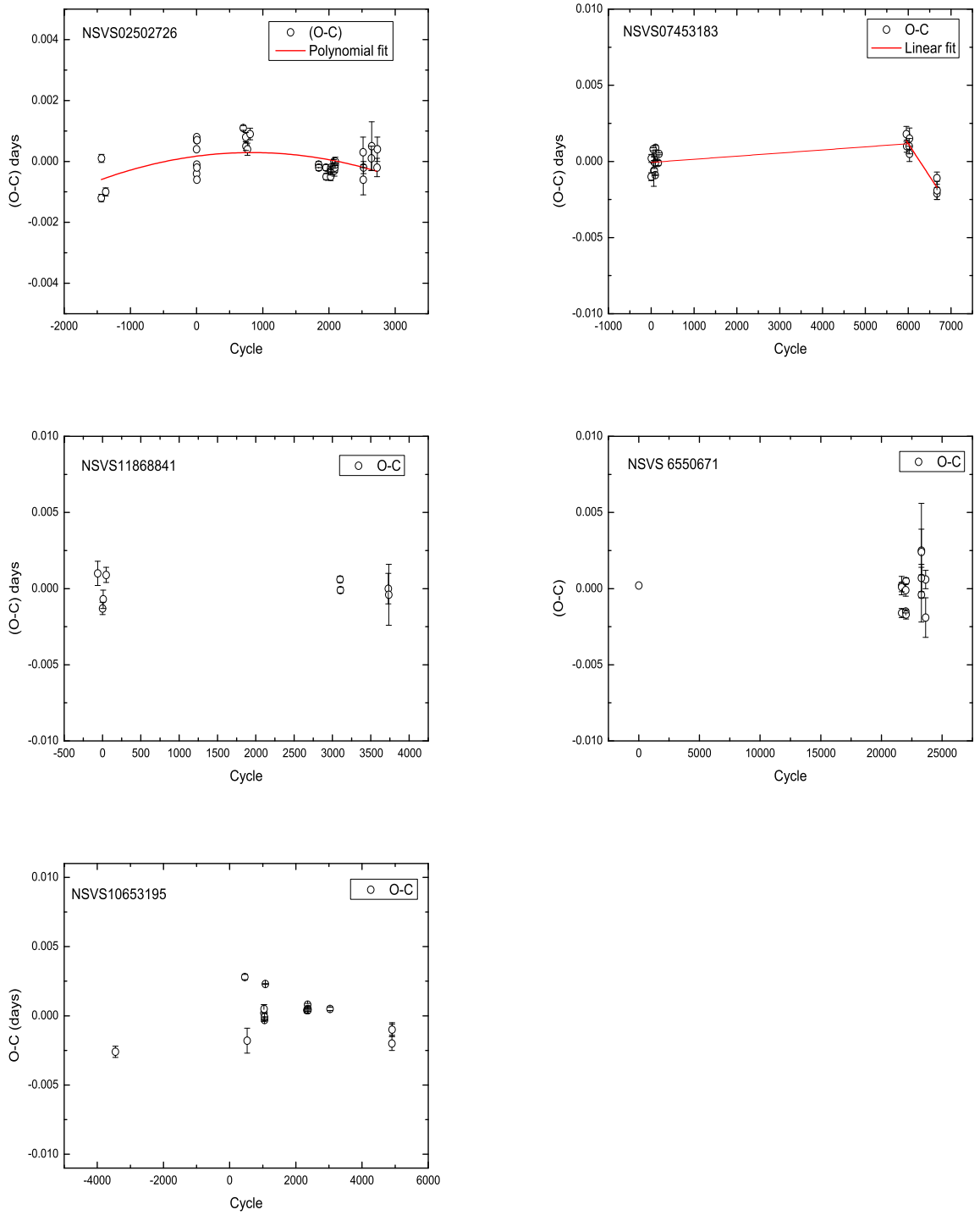

Figure 3. (O−C) diagram for the five low-mass eclipsing binaries. The solid line represents the polynomial fit.

LCs. This may be a viable way to obtain a proper solution (Zhang & Zhang 2007, related reference). For each assumed value of q, the LCs in different bands were simultaneously solved based on mode 2 (detached mode). We obtained the solutions for all the assumed mass ratios from several runs. The relationship between the sum of the weighted square deviation ($\Sigma\ (O-C)_i^2$) and the mass ratios of NSVS 07453183 and NSVS 10653195 are illustrated in Fig. 4, where the lowest values are found to be about 0.6 for NSVS 07453183 and 0.25 for NSVS 10653195, respectively.

Because there were no spectroscopic components, especially spots on the quadratures, it was difficult to tell whether spots were located on the primary or secondary components (Zhang & Gu 2007; Zhang et al. 2010a). Therefore, we assumed that the spots were on the surface of the primary. Moreover, it is reasonable to

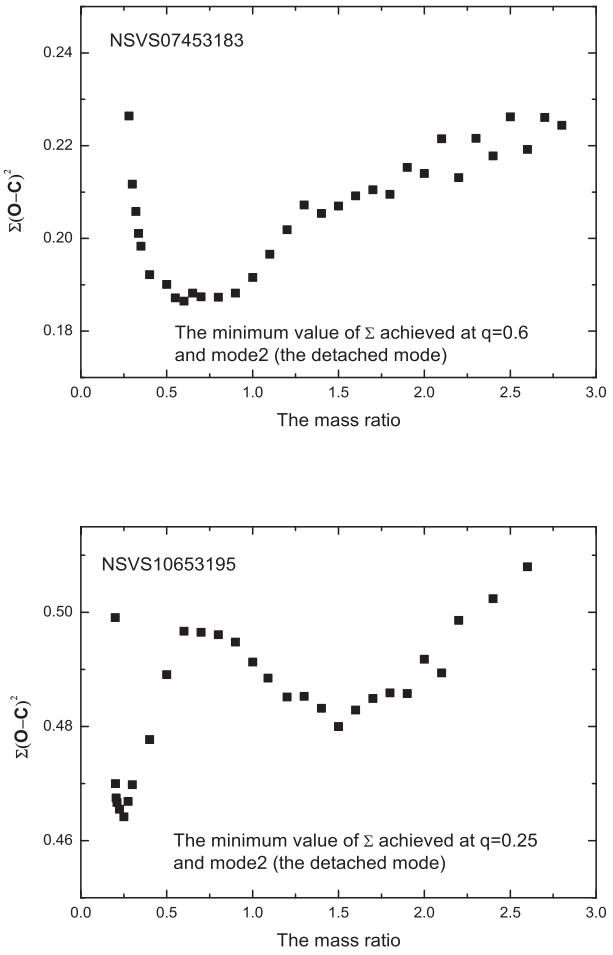

Figure 4. The relation between the sum of the squares of the residuals and the mass ratio q of NSVS 07453183 and NSVS 10653195.

fix the spot latitude, since the spot area and the latitude are highly correlated with its temperature and radius, respectively. The star-spot temperature is based on measurements from a simultaneous modelling of high-precision, absolutely calibrated, multibandpass photometric data, Doppler imaging result, modelling of molecular bands and atomic line-depth ratio (Berdyugina 2005; Strassmeier 2009). The latter is the most accurate method. The current precision of the photometric observation (about 0.01 mag) does not enable reliable determination of the temperature of spots (Eker 1999). Moreover, the determination of a star-spot temperature is always mathematically correlated with the determination of the star-spot size. Therefore, it is reasonable to explain the LC evolution by not varying spot temperatures but rather, focusing on effective spot sizes and longitudes. Here, the latitude of the spot is assumed to be at 90°, which means that spot centres are on the equator of the component. The longitude of the star-spot centre is measured counterclockwise (as viewed from above the $+Z$-axis) from the line of the star centre, from 0 to 2π rad. Thus, in this paper, it has been transformed to a binary orbital motion notation.

The adjustable orbital parameters used in differential correction calculations are the orbital inclination i, the temperature of the secondary T_2, the dimensionless potentials of the two components Ω_1 and Ω_2, the orbital separation of the mass centre of the two components (a), and the monochromatic luminosity of the primary L_1 deriving from the approximate Kurucz atmosphere model option of the WD program (Kurucz 1993). The preliminary values of these orbital parameters were taken from the prior photometric solutions (see Table 1). After a great many runs (a single run allows us to enter into the preliminary parameters, that eventually results in a more reliable outcome.), the orbital solutions were derived (Table 7). For NVSV 06550771, the detached (Mode 2 in WD program) was first used to check whether the surface potential of the components reached their Roche limits or not. After trials, it was found that the primary component filled its Roche lobe. Thus, we changed mode 2 (detached system) to mode 4 (semi-detached system) for NVSV 06550771 consistent with the results derived by Dimitrov & Kjurkchieva (2010). Our new star-spot parameters along with published results obtained by other astronomers are listed in Table 8. The errors of our obtained parameters came from the covariance matrix of the least-squares fit. The theoretical and observed LCs are shown in Fig. 5, and corresponding configurations are shown in Fig. 6.

We collected seven LCs published by Coughlin & Shaw (2007), Çakirli et al. (2009) and Lee et al. (2013). When comparing the LCs with each other, we found that there are variations on the shapes (in Figs 1 and 7). This indicates that the LCs are variable over several years for NSVS 02502726, NSVS 07453183, NSVS 11868841, NSVS 06550671 and NSVS 10653195. To study an evolution of star-spots on these systems, we attempt to derive the spot parameters for the collected LCs on the basis of our new photometric solution. Because the spot area is highly correlated with its temperature and the latitude is highly correlated with its radius, it is reasonable to only adjust one of the three spot parameters. Hence, we assumed that the spot latitude and temperature did not change and we only adjusted the spot longitude and radius. At the same time, we also adjusted the luminosity of the primary L_1 because we used different telescopes and comparison stars. After several runs, we derived star-spot parameters. The results are listed in Table 8, the theoretical and observed LCs are shown in Fig. 7.

4.2 The chromospheric activity analysis

The Hβ and Hγ lines are useful diagnostic indicators of chromospheric activity for late-type stars in the middle chromosphere (e.g. Gunn & Doyle 1997; Montes et al. 1997,2004; Zhang & Gu 2008; Zhang 2011). The emissions at cores of these lines are the traditional behaviour of chromospheric activity. Our normalized spectra of NSVS 07453183 and NSVS 10653195 were analysed by the spectral subtraction technique using the program, STARMOD (Barden 1985; Montes et al. 1995). In this method, we constructed the synthesized spectra from artificially rotationally broadened, radial-velocity shifted, and the weighted spectra of the two inactive stars with the same spectral type and luminosity class as two components of the active systems. The intensity weights for spectral subtraction were obtained from photometric LC modelling, which was also used to discuss the chromospheric activity of the eclipsing binary ER Vul by Gunn & Doyle (1997). We used the inactive star HR 2458 as a template for NSVS 07453183 and NSVS 10653195. The synthesized and subtracted spectra (the observed spectra minus the synthesized one) are shown in Fig. 2. We calculated the equivalent widths (EWs) and the full width at half-maximum of the Hβ and Hγ lines, which were evaluated on the subtracted spectra by integrating them over the emission profile using an IRAF SPLOT task. These parameters confirmed the chromospheric activity of NSVS 07453183 and NSVS 10653195. The results are listed in Table 9. Usually the short-period eclipsing binaries rotate quite

Table 7. The results of orbital parameters for the five low-mass eclipsing binaries.

Element	NSVS 10653195	NSVS 07453183	NSVS 11868841	NSVS 02500276	NSVS 06550671	NSVS 06550671
Date	2012 April	2011 March	2011 October	2011 Jan	2011 Feb 1	2011 Feb 1
Method	Light	Light	Light + radial	Light + radial	Light + radial	Light + radial
Mode	Detached	Detached	Detached	Detached	Detached	Semi-detached
Orbital period (d)	0.5607	0.3670	0.6018	0.5598	0.1926	0.1926
T_1	4120 K a	3570 K a	5250 K a	4300 K a	3735 K a	3735 K a
a ($R_\odot$)	–	–	3.43 ± 0.05	2.85 ± 0.026	1.27 ± 0.02	1.33 ± 0.03
γ(kms^{-1})	–	–	-78.0 ± 1.6	8.4 ± 2.0	0.8 ± 2.0	-1.4 ± 2.0
$M1$ ($M_\odot$)	–	–	0.886 ± 0.035	0.685 ± 0.042	0.494 ± 0.042	0.578 ± 0.04
$M2$ ($M_\odot$)	–	–	0.616 ± 0.024	0.310 ± 0.020	0.249 ± 0.021	0.280 ± 0.02
$R1$ ($R_\odot$)	–	–	1.01 ± 0.02	0.67 ± 0.01	0.54 ± 0.01	0.59 ± 0.01
$R2$ ($R_\odot$)	–	–	0.96 ± 0.02	0.74 ± 0.01	0.18 ± 0.01	0.27 ± 0.01
q	0.280 ± 0.004	0.601 ± 0.007	0.695 ± 0.002	0.453 ± 0.004	0.504 ± 0.008	0.484 ± 0.014
i	$87.^\circ079 \pm 0.^\circ130$	$84.^\circ305 \pm 0.^\circ113$	$88.^\circ93 \pm 0.^\circ047$	$86.^\circ72 \pm 0.^\circ05$	$74.^\circ58 \pm 0.^\circ38$	$66.89 \pm 0.^\circ45$
T_2	4064 ± 4 K	3438 ± 6 K	5055 ± 4 K	3830 ± 2 K	3313 ± 19	3359 ± 28
Ω_1	4.612 ± 0.033	4.032 ± 0.044	4.141 ± 0.007	4.754 ± 0.032	2.972 ± 0.02	2.83 a
Ω_2	2.722 ± 0.018	3.156 ± 0.020	3.692 ± 0.006	3.060 ± 0.013	4.893 ± 0.086	3.689 ± 0.092
$L_{1V}/(L_1+L_2)_V$	0.5679 ± 0.0024	0.5494 ± 0.0037	0.5807 ± 0.0008	0.6558 ± 0.001	0.9559 ± 0.0001	0.9148 ± 0.0005
$L_{1R}/(L_1+L_2)_R$	0.5713 ± 0.0023	0.5437 ± 0.0036	0.5699 ± 0.0008	0.6251 ± 0.002	0.9545 ± 0.0001	0.9097 ± 0.0006
$L_{1I}/(L_1+L_2)_I$	0.5670 ± 0.0023	0.5179 ± 0.0039	0.6077 ± 0.0007	0.5785 ± 0.002	0.9430 ± 0.0001	0.8926 ± 0.0007
r_1(pole)	0.2305 ± 0.0018	0.2894 ± 0.0037	0.3152 ± 0.0004	0.2318 ± 0.0017	0.3993 ± 0.0032	0.4169 ± 0.0023
r_1(point)	0.2338 ± 0.0019	0.3052 ± 0.0047	0.3446 ± 0.0006	0.2365 ± 0.0019	0.4854 ± 0.0111	0.5739 ± 0.0068
r_1(side)	0.2323 ± 0.0018	0.2953 ± 0.0040	0.3244 ± 0.0005	0.2340 ± 0.0018	0.4212 ± 0.0041	0.4430 ± 0.0027
r_1(back)	0.2333 ± 0.0019	0.3015 ± 0.0044	0.3358 ± 0.0005	0.2358 ± 0.0019	0.3359 ± 0.0053	0.4709 ± 0.0026
r_2(pole)	0.2025 ± 0.0032	0.3006 ± 0.0034	0.2189 ± 0.0003	0.2493 ± 0.0020	0.1380 ± 0.0033	0.1979 ± 0.0076
r_2(point)	0.2206 ± 0.0049	0.3675 ± 0.0108	0.2281 ± 0.0003	0.2792 ± 0.0036	0.1397 ± 0.0035	0.2067 ± 0.0093
r_2(side)	0.2064 ± 0.0035	0.3123 ± 0.0040	0.2216 ± 0.0003	0.2558 ± 0.0023	0.1385 ± 0.0033	0.2002 ± 0.0080
r_2(back)	0.2163 ± 0.0044	0.3375 ± 0.0057	0.2262 ± 0.0003	0.2701 ± 0.0029	0.1395 ± 0.0034	0.2050 ± 0.0089
$\sum(O-C)_i^2$	0.4393	0.1112	0.037	0.1273	0.0754	0.0966

Notes. Parameters not adjusted in the solution are denoted by a mark 'a'.

fast. For GSC 2314−0530, the rotational velocities of the primary and secondary components were 145 and 69 km s^{-1}, respectively (Dimitrov & Kjurkchieva 2010). They had very wide spectra. Because the resolution of our spectra was about 4000, the spectral lines of the primary and secondary were blended. We could not determine the activity levels for each stellar component of the binaries. The chromospheric emissions represent the components of the eclipsing binary.

5 DISCUSSIONS AND CONCLUSION

We have presented the new 15 CCD V, R and I LCs of the five low-mass eclipsing binaries (NSVS 02500276, NSVS 07453183, NSVS 11868841, NSVS 06550671 and NSVS 10653195), and two spectra of the NSVS 06550671 and NSVS 10653195. The cases are discussed and summarized as follows.

5.1 The flare event

Flares are known as sudden and violent events that release magnetic energy and hot plasma from the stellar atmosphere, which are detected on magnetically active stars. However, in our studies, no flare activity was observed on NSVS 07453183. As can be seen from Fig. 1, a flare event appeared around phase 0.39 on 08/12/2011 (HJD 2455904.3064). In order to demonstrate that, we calculated the residuals between the observations and theoretical values (displayed in Fig. 8). The flare duration was found to be 116 min (phase 0.33–0.55) and the time required for the flare to peak was about 32 min. Thus, it can be assumed that the brightness decayed slowly after the initial rapid flaring. The maximum amplitudes of the flare were 0.1 mag in V, 0.076 mag in R and 0.05 mag in I band (Fig. 8). The flare might have been located on the primary component since it occurred around phase 0.33–0.55, when most the secondary was eclipsed. NSVS 07453183 was monitored photometrically for a total of 26.6 h. It seems that the flare rate of NSVS 07453183 might have been 0.0375 h^{-1}, but more data is needed to confirm this. Similar flare events have also been reported for other low-mass eclipsing binaries such as CU Cnc (Qian et al. 2012), CM Dra (Lacy 1977; Kim et al. 1997; Kozhevnikova et al. 2004; Nelson 2007), DV Psc (Zhang et al. 2010a), NSVS 06550671 (Dimitrov & Kjurkchieva 2010), V405 And (Vida et al. 2009) and YY Gem (Doyle et al. 1990). For NSVS 06550671, we found no flare events during our observational runs, and this indicates that it might have been stable in the studied time period. However, Dimitrov & Kjurkchieva found six flares on NSVS 06550671 in 2009 (Dimitrov & Kjurkchieva 2010), which revealed its high flare activity at the time of the study. So far, NSVS 06550671 has been monitored photometrically for 22.74 h by us and 31.93 h by Dimitrov & Kjurkchieva (2010). The updated flare rate of NSVS 06550671 is about 0.11 flares h^{-1}, which is larger than most of the other binaries (Table 10), e.g. 0.0386 flares h^{-1} of CM Dra (Lacy 1977; Metcalfe et al. 1996; Kim et al. 1997; Kozhevnikova et al. 2004; Nelson & Caton 2007) and 0.05 of CU Cnc (Qian et al. 2012).

Table 8. The star-spot parameters for the five eclipsing binaries (including the published data).

Star(NSVS)	$T(24,+)$	Loc	Latitude	Longitude	Radius	Temperature	Loc	Latitude	Longitude	Radius	Temperature	$\sum_i(o-c)$	Factor	Ref
02502726	53692.0	P	30	22	30	4152	P	5	284	32	4152		3.11 per cent	1
02502726	54499.0	P	37	254	38	3655 a	S	39	261	54	2824		10.1 per cent	2
02502726	54499.0	P					S	22	141	57 1	3403		10.1 per cent	2
02502726	54499.0	P	90a	114.6 ± 0.1	22.8 ± 0.2	3115 a	P	90 a	254.5 ± 0.5	18.5 ± 0.1	2661 a	0.919	2.80 per cent	6*, 2
02502726	53692.0	P	90a	70.7 ± 0.5	10.5 ± 2.6	3115 a	P	90 a	255.7 ± 6	11.6 ± 3.1	2661 a	0.96	0.82 per cent	6*, 1
02502726	54928.1	P	90a	49.2 ± 2.5	15.8± 4.5	3115 a	P	90 a	291.8 ± 4.1	14.9 ± 2.0	2661 a	0.958	1.56 per cent	6*, 7
02502726	55650.3	P	90a	69.7 ± 0.3	20.1± 0.6	3115 a	P	90 a	275.7 ± 0.5	19.0 ± 0.1	2661 a	0.919	2.52 per cent	6*, 7
02502726	54928.1	P	25.1	39.5	49.4	4080	S	91.4	296.8	33.5	3507			7
02502726	55650.3	P	17.5	33	64.1	4080 a	S	96.5	267.9	35.2	3545			7
02502726	54499.0	P	34.5	118.4	36.2	3521	S	77	263.6	37	3392			7*,2
02502726	55528.8	P	90a	68.3 ± 0.4	19.9± 0.2	3115 a	P	90 a	283.8 a	23.2 ± 0.1	2661 a	0.230	3.18 per cent	6
02502726	55592.3	P	90a	87.4 ± 0.8	19.5± 0.3	3115 ± 103	P	90 a	283.8 ± 0.4	18.6 ± 0.2	2661 ± 172	0.127	2.43 per cent	6
02502726	55907.7	P	90a	86.8 ± 2.4	16.4± 1.0	3115 a	P	90 a	254.5 ± 0.8	17.9 ± 0.2	2661 a	0.266	2.00 per cent	6
02502726	55977.1	P	90a	83.5 ± 1.4	18.8± 1.4	3115 a	P	90 a	234.1 ± 1.7	12.3 ± 0.5	2661 a	0.324	1.65 per cent	6
02502726	56023.6	P	90a	82.4 ± 6.9	15.8± 2.8	3115 a	P	90 a	248.3 ± 1.7	19.3 ± 0.3	2661 a	0.266	2.13 per cent	6
07453183	53476.2	P	31	29	21	2963	P	55	332	79	3499		2.99 per cent	1
07453183	53476.2	P	90a	62 ± 2	15.1 ± 0.3	2437 a	S	90 a	335 ± 3.4	15.8 ± 2	2802±172	0.709	0.97 per cent	6*, 1
07453183	55644.1	P					P	90 a	227.3 ± 5.7	17.9 ± 0.9	2569 ± 273	0.1112	0.86 per cent	6
07453183	55668.6	P					P	90 a	227.9 ± 2.3	18.0 ± 2.4	2569 ± 659	0.6901	0.87 per cent	6
07453183	55904.7	P					P	90 a	257.6 ± 2.8	13.5 ± 5.5	2871 ± 542	0.3178	0.39 per cent	6
11868841	53658.2	P	172	22	50	3412	P	1	137	60	4148		19.3 per cent	1,3
11868841	53658.2	P	90 a	52.4 ± 3.4	14.9 ± 1.9	4472 a ±	P	90 a	305.9 ± 1.5	23.2± 1	4328a ±	0.324	2.12 per cent	6*,1
11868841	55528.6	P	90 a	98.26 ± 1.6	21.0 ± 8.7	4472 ± 322	P	90 a	228.2± 1.7	13.5± 1.5	4328 ± 334	0.037	1.30 per cent	6
11868841	55909.0	P	90 a	61.55 ± 9.0	13.0 ± 4.6	4472 a ±	P	90 a	267.1 ± 8.7	15.1± 0.9	4328a ±	0.088	0.86 per cent	6
06550671	–	P	70±10	147 ± 5.0	20 ± 1	3175 ± 50	P	75±10	195±5	8 ± 1	3175 ± 50		1.48 per cent	5
06550671	55594.0	P					P	90 a	233 ± 6	23 ± 8	3550 ± 149	0.0966 Semi	0.64 per cent	6
06550671	55594.0	P					P	90 a	229 ± 2	21 ± 2	3550 ± 21	0.075	0.57 per cent	6
06550671	55905.1	P					P	90 a	236 ± 10	19 ± 4	3550 a	0.0815	0.47 per cent	6
06550671	55590.0	P					P	90 a	230 ± 1	21 ± 1	3550 ± 21	0.026	0.57 per cent	6
06550671	55525.1	P					P	90 a	219 ± 1	21 ± 1	3550 ± 21	0.109	0.57 per cent	6
10653195	53867.8	P	161	44	87	3832	P	68	157	70	4038		9.12 per cent	1
10653195	2008/05	S	90	115	50	3710	P	150	155	50	3528		3.40 per cent	4
10653195	53867.8	P					P	90 a	272.9 ± 2.2	19.6 ± 1.6	3179 ± 247	0.4393	1.05 per cent	6
10653195	56021.8	P	90 a	1.2 ± 2.1	14.2 ± 0.8	3179 a	P	90 a	272.9 ± 5	18.7 ± 3	3179 a	0.492	1.14 per cent	6*,1

Reference (1) Coughlin & Shaw 2007, (2) Çakirli et al. 2009, (3) Çakirli et al. 2010, (4) Wolf et al. 2010, (5) Dimitrov & Kjurkchieva 2010, (6) present paper, (7) Lee et al. 2013, P: the primary component, S: the secondary component. Parameters not adjusted in the solution are denoted by a mark 'a'. * means that the results derived for published data. Loc means location of star-spot.

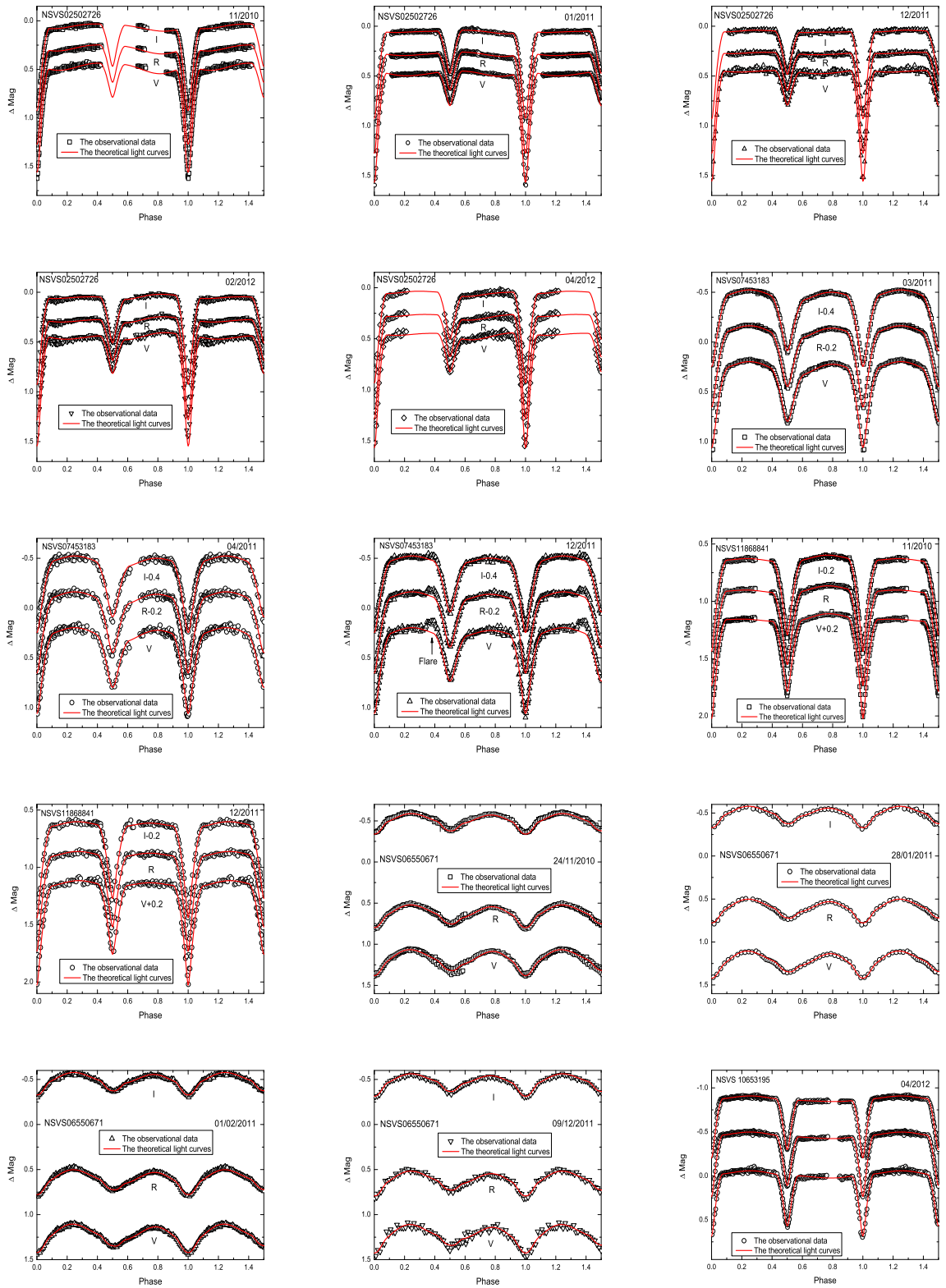

Figure 5. The observational and theoretical LCs of the five low-mass eclipsing binaries. The points and solid lines represent the observational and theoretical LCs, respectively.

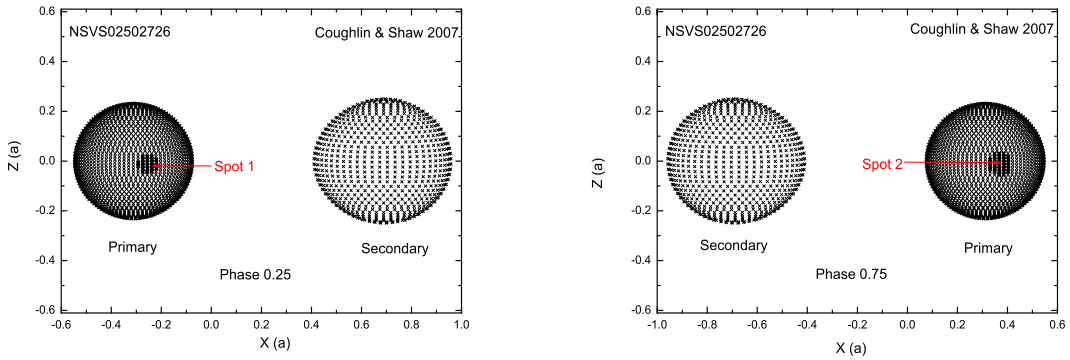

Figure 6. The configurations of the five low-mass eclipsing binaries. *X* represents the line perpendicular to the line of sight in orbital plane of eclipsing binary. *Z* represents the normal direction of the orbital plane of the binary. The unit (a) is the orbital separation of the mass centre of the two components. This figure is available as online material.

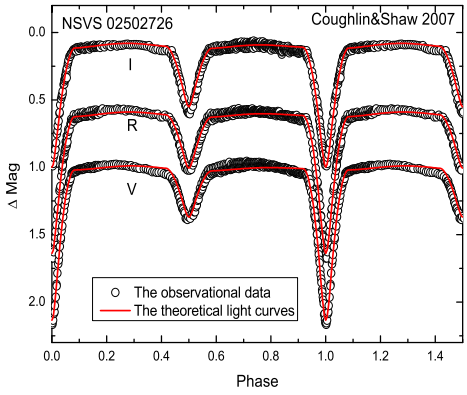

Figure 7. All the collected published LCs and their corresponding theoretical LCs based on our new orbital parameters. This figure is available as online material.

Table 9. The parameters of chromospheric active indicators.

Star name	Hγ			Hβ		
	SN	EW (Å)	FWHW (Å)	SN	EW (Å)	FWHW (Å)
NSVS 06550671	22	2.3 ± 0.4	8.5 ± 1.5	25	2.5 ± 0.5	6.76 ± 0.2
NSVS 10653195	27	1.7 ± 0.2	4.9 ± 0.2	34	2.5 ± 0.3	8.4 ± 4.5

5.2 Orbital parameters and star-spot parameters

Our studies reveal remarkable distortions of the LCs of the five low-mass eclipsing binaries, which suggests the presence of high-level surface activity on these system components. We have presented reasonable explanations for these, which have been based on star-spot due to magnetic activity. Our new orbital parameters of the inclination, the effective temperatures of the secondary, and the contribution of the primary component are similar to those derived by previous authors (Coughlin & Shaw 2007; Çakirli et al. 2009, 2010; Dimitrov & Kjurkchieva 2010). The mass ratios of NSVS 11868841, NSVS 02502726 and NSVS 06550671 are similar to those derived by Çakirli et al. (2009, 2010) and Dimitrov & Kjurkchieva (2010). However, the mass ratios of the NSVS 07453183 and NSVS 10653195 are different from the previous results (Coughlin & Shaw 2007). These observations should be confirmed by further spectroscopic results.

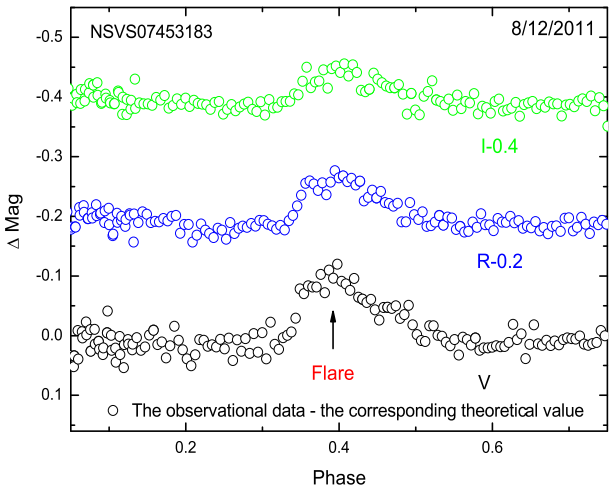

Figure 8. The flare of NSVS 07453183 in *V*, *R* and *I* bands. The data represent the difference of the observational data and their corresponding theoretical value.

The absolute parameters of NSVS 02502726, NSVS 11868841 and NSVS 06550671 were analysed together with our new CCD LCs and the published radial velocity curves (Çakirli et al. 2009, 2010; Dimitrov & Kjurkchieva 2010). Using our new physical parameters of these low-mass eclipsing binaries, we checked the evolutionary state of these systems in a mass–radius diagram with a mass range of 0.1–1.0 $m_{\odot}$ (Fig. 9). We displayed the parameters of NSVS 02502726, NSVS 11868841 and NSVS06550671 as □, ○, △, respectively. The components of each binary are connected with a light line and the different colours represent the different results derived by different authors (Çakirli et al. 2009, 2010; Dimitrov & Kjurkchieva 2010; Lee et al. 2013). In order to compare the observed parameters with the theoretical physical parameters, we also plotted the predicted values of the stellar evolutionary models with the solar metallicity derived by Baraffe et al. 1998, and the dashed lines represent the isochrones from the Baraffe et al. (1998) models with log ages = 7.0, 7.1, 7.2 and 7.8 yr, respectively. Further, we also portray the experienced mass–radius relationship of Bayless & Orosz (2006) by a solid line. The primary components of NSVS 02502726, NSVS 11868841 and NSVS06550671 (semi-detached model) are consistent with the previous observational and theoretical values of low-mass eclipsing binaries. The radii of the

Table 10. The flare ratio of the binaries.

Name	Spectral type	Rotation period	Flare	Flare ratio (h^{-1})	Reference
DV Psc	K 4V+M	0.308 536 41	6	0.082	Zhang et al. (2010a), Pi et al. (2014)
CU Cnc	M 3.5V	2.771 468	4	0.05	Qian et al. (2012)
GSC 2314−0530	M dwarf	0.192 636	6	0.11	Dimitrov & Kjurkchieva (2010), our study
V471 Tau	K2V+WD	0.521 18345	7	0.029	Kamiński et al. (2007)
CM Dra	M dwarf	1.268 3897	6	0.057	Nelson & Caton (2007)
CM Dra	M dwarf	1.268 3897	1	0.05	Lacy (1977)
CM Dra	M dwarf	1.268 3897	1	0.02	Metcalfe et al. (1996)
CM Dra	M dwarf	1.268 3897	1	0.04	Kim et al. (1997)
CM Dra	M dwarf	1.268 3897	4	0.026	Kozhevnikova et al. (2004)
EC13471−1258	M 3.5-M4	0.150 69	2	0.067	O'Donoghue et al. (2003)
YY Gem	Dme	0.814 2822	5	0.735	Doyle et al. (1990)
YY Gem	Dme	0.814 2822	22	0.22	Doyle & Mathioudakis (1990)
YY Gem	Dme	0.814 2822	12	0.265	Moffett & Bopp (1971)
DI Peg	Dme	0.711 817	2	0.13	Chaubey (1980)
NSVS 07453183	M2	0.366 971	1	0.0375	Our study

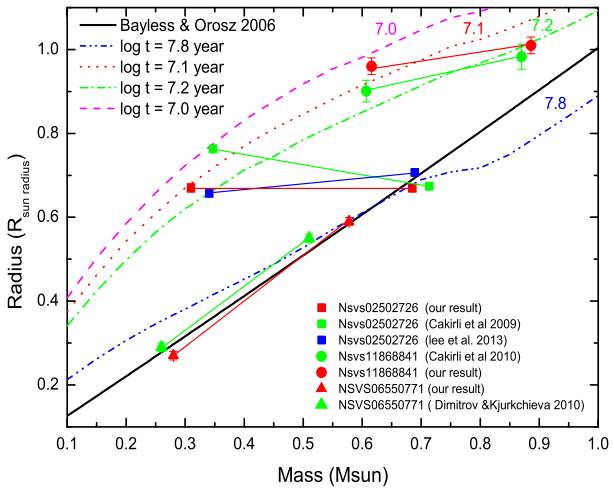

Figure 9. The mass–radius diagram of the detached eclipsing binaries with mass range 0.2–1.0 $M_{\odot}$. The orbital results of NSVS 02502726, NSVS 11868841 and NSVS06550671 are displayed as □, ○; and △, respectively. The components of each binary are connected with a light line and different colours represent the results derived by different authors. The solid line corresponds to the empirical mass–radius relation of Bayless & Orosz (2006) and the dashed lines represent the isochrones from the Baraffe et al. (1998) models with log ages = 7.0, 7.1, 7.2, 7.8 yr, respectively.

secondary component of NSVS 02502726 and NSVS 11868841 are larger than those predicted by the stellar theory (Baraffe et al. 1998). From this figure, we found a best-fitting age of the secondary component of NSVS 02502726 as 126 myr and the secondary component of NSVS 11868841 as 112 myr, thus indicating that they are younger than their corresponding primary components. Using their mass and radius, we determined that both the secondary components of the NSVS 02502726 and NSVS 11868841 were in the stages of the pre-main-sequence contraction. Our results are consistent with those derived by Çakirli et al. (2009, 2010) and Lee et al. (2013).

5.3 The star-spot evolution

Decades of the continuous photometric monitoring of RS Cvn stars revealed that, according to many astronomers, the spot tends to occur around the quadrature longitudes (90°and 270°) forming two active

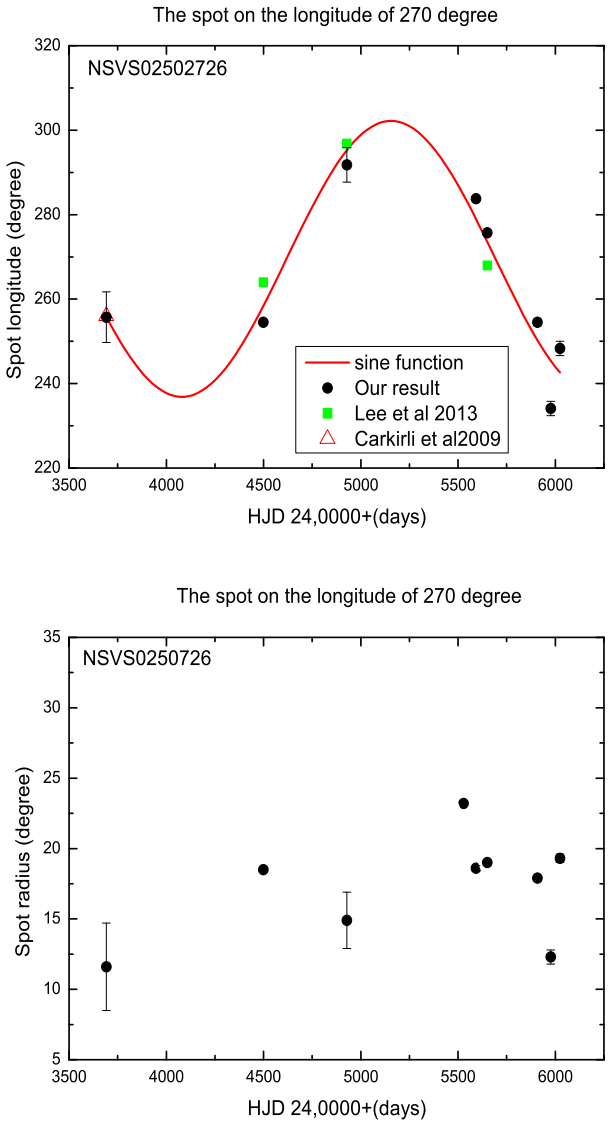

Figure 10. The spot evolution of NSVS 02502726. Different points represent the result derived by different authors. The solid line represents the fit with the sine function.

longitude belts (Zeilik et al. 1988, 1989, 1994; Olah et al. 1989; Henry et al. 1995; Lanza et al. 2001; Lanza, Catalano & Rodonò 2002; Çakirli et al. 2003; etc.). The active longitudes are permanent but can continuously migrate in the orbital reference frame (Berdyugina & Tuominen 1998). There is periodic switching of the dominant activity from one active longitude to the other (flip-flop cycle; Berdyugina & Tuominen 1998). There was a mechanism based on an oscillating quadrupole type mode and a steady, mixed-polarity non-axisymmetric mode to explain them (Moss 2004). Considering that the most reliable star-spot parameter determined by the traditional LCs method is active-region longitude (Berdyugina 2005), we studied the star-spot evolution of the five low-mass eclipsing binaries based on their star-spot longitudes. When comparing the star-spot longitudes in different seasons, our results are different from those previously obtained results (see Table 8). For the evaluation of the total distortion of the LCs, Pribulla et al. (2000) introduced a dimensionless factor, which was defined as the ratio between the luminosity blocked by spots and the total luminosity of an unspotted binary. The calculated resulting spot factors are listed in Table 8. The spot factors of the five low-mass eclipsing binaries changed over the course of several years. The LC variations of NSVS 10653195, NSVS 07453183 and NSVS 11868841 are presented here. The spot evolutions of several years have also been found on several other low-mass eclipsing binaries, such as ASAS-09 and ASAS-21 (Helminiak, Konacki & Zloczewski 2011), GU Boo (Windmiller, Orosz & Etzerl 2010), NSVS 06507557 (Coughlin & Shaw 2007) and YY Gem (Torres & Ribas 2002). For NSVS 02502726, the radius of spots within the longitude region around 180°–360° suggests that its activity is also variable over several months (see Fig. 1). Such a short-term variation of several months was also found on other low-mass eclipsing binaries, e.g. NSVS 065007557 (Coughlin & Shaw 2007) and K10200948 (Harrison et al. 2012). However, the position of spot within the longitude around 90° suggests that the activity is stable in short time-scale of two months. Moreover, the star-spot longitudes and factors of NSVS 07453183 and NSVS 06550671 are stable on a short time-scale of several months. Therefore, the star-spot of NSVS 07453183 and NSVS 06550671 can be considered to be quite stable over several months.

The longitude of the spots has been checked for a possible magnetic cycle around the quadrature position (Pribulla et al. 2000; Rodonò et al. 2000; Dal, Sipahi & Özdarcan 2012). The similar functions (the quadratic trend combined with sine waves or quasi-sinusoidal variation) were also used to search the magnetic cycles of RT And (Pribulla et al. 2000), II Peg (Rodonò et al. 2000) and GSC 02038−0293 (Dal et al. 2012). For NSVS 02502726, the star-spot position within a longitude region of 180°–360° was found to be variable (see Fig. 10). To examine its activity cycle, a sinusoidal function ($y = y0 + A \times \sin(w \times x + a)$) analysis was performed using the least-squares method, which led to the following equation:

$$\text{Spot Longitude (degree)} = 269.5(3.1)$$
$$+32.7(3.5) \times \sin(0.0029(0.0001) \times t + 7.2(0.2)). \quad (2)$$

The result is displayed in Fig. 10. The sinusoidal term of the above equation reveals a periodic oscillation with an amplitude of 32.°7(3.°5). Using $T = 2\pi/(365^{*}\omega)$ (yr), where ω is the coefficient of t in days, the magnetic cycle is 5.9(±0.2) yr resembling the activity of the Sun (Berdyugina & Usoskin 2003). For close binaries with cool active components, the magnetic activity cycles are suggested to be associated with the variation of the orbital period (Hall 1989). The relationship between the orbital period modulation and the star-spot cycle has been discussed by previous authors (Applegate 1992; Keskin et al. 1994; Rodonò, Lanza & Catalano 1995; Lanza, Rodonò & Rosnor 1998a; Lanza et al. 1998b). For NSVS 02502726, we found there is a weak period variation (Fig. 3). However, the time span covered by the available data is insufficient for us to draw any definite conclusion (the connection between magnetic activity and orbital period variation). According to Rudiger, Elstner & Ossendrijver (2003), the cyclic stellar activity is always most possibly associated with strong internal differential rotation. The star-spot preferred longitudes can be explained by tidal effects on the dynamics of magnetic flux tubes, which are thought to give rise to star-spots as they emerge on the stellar surface (Holzwarth & Schüssler 2002). In addition, the total spotted area can also be used as an index of the overall magnetic activity (Lanza et al. 1998b). There are variations in the spot radius for NSVS 02502726 on the secondary quadratures (see Fig. 10). The radius of the secondary of NSVS 02502726 is smaller than that found by Çakirli et al. (2009). It is to be noted that the LC distortions of ours and Lee et al. (2013) are weaker than those of Çakirli et al. (2009). The variation in the spot radius may be caused by star-spot evolution.

5.4 Period variation of low-mass eclipsing binaries

To clarify the period change, we considered the possibility of orbital period variation by analysing the minima times of NSVS 02502726, NSVS 07453183, NSVS 11868841, NSVS 06550671 and NSVS 10653195. The (O−C) diagrams suggest the possible decrease of period for NSVS 02502726. Our analysis of NSVS 02502726 suggests a weak continuous secular decrease of the period at the rate of $dp/dt = -2.1(0.8) \times 10^{-7}$ d yr^{-1}, which is smaller than the result of Lee et al. (2013). On the one hand, the period variation may be caused by mass transfer from the primary component (more massive) to the secondary one (less massive). On the other hand, the period decrease might be due to magnetic braking (e.g. Applegate 1992; Lanza et al. 1998a). For NSVS 07453183, we found sudden jumps in the orbital period. Period jumps are a fairly common phenomenon in close binaries, although the physical mechanism for the period jump is not well known. There are several hypotheses to explain the sudden period changes (Li & Zhang 2006). These include the mass ejection from the star-spots and then mass transfer and subsequent angular momentum release (Helt 1987), the variation of the structure of the convective envelope (Qian 2002), and the mass-loss or mass accretion from the circumstellar matter (Scaltriti et al. 1993). Moreover, the time spans of O−C residual of these low eclipsing binaries are around less than 10 years, and also there is also an observational gap. Therefore, it is too early to decide the characteristics of the periodic variation, and future photometric monitoring observations are needed for confirmation.

5.5 Chromospheric activity of NSVS 06550671 and NSVS 10653195

Prior to our new observations, there was no information about the behaviour of the chromospheric activity indicators (the Hβ and Hγ lines) of NSVS 10653195 and NSVS 06550671. In the present study, we can see from the observed spectra of NSVS 06550671 and NSVS 10653195 that the chromospheric activity indicators of the Hβ and Hγ lines show strong filled-in absorption with self-reversal core emissions (Fig. 2). The subtraction spectra reveal that the cores of these lines exhibit excess emissions. All this indicates that the chromospheres of NSVS 06550671 and NSVS 10653195

are active, which may originate the plage-like regions. For NSVS 06550671, our results are consistent with the Hα emission derived by Dimitrov & Kjurkchieva (2010).

ACKNOWLEDGEMENTS

The authors would like to thank the observing assists at the 85 cm and 2.16 m telescope of Xinglong station for their help during the observations. We also thank their kind help and support during the visit to Research Group for Compact Objects and Diffuse Medium, NAOC. We would also like to thank the anonymous referee for his (her) valuable comments, which led to significant improvement in the manuscript. This work is partly supported by GuiZhou natural Science Foundation no. 20092263 and supported partly by the Joint Fund of Astronomy of the National Natural Science Foundation of China (NSFC) and the Chinese Academy of Sciences (CAS) grant no. 10978010, 11263001 and U1231102. This work was partially Supported by the Open Project Program of the Key Laboratory of Optical Astronomy, NAOC, CAS. This research has made use of the SIMBAD data base, operated at CDS, Strasbourg, France.

REFERENCES

Applegate J. H., 1992, ApJ, 385, 621
Banfi M. et al., 2012, Inf. Bull. Var. Stars, 6033, 1
Baraffe I., Chabrier G., Allard F., Hauschildt P. H., 1998, A&A, 337, 403
Barden S. C., 1985, ApJ, 295, 162
Bayless A. J., Orosz J. A., 2006, ApJ, 651, 1155
Berdyugina S. V., 2005, Living Rev. Sol. Phys., 2, 8
Berdyugina S. V., Tuominen I., 1998, A&A, 336, 25
Berdyugina S. V., Usoskin I. G., 2003, A&A, 405, 1121
Blake C. H., Torres G., Bloom J. S., Gaudi B. S., 2008, ApJ, 684, 635
Çakirli Ö., Ibanoğlu C., Djurašević G., Erkapić S., Evren S., Taş G., 2003, A&A, 405, 733
Çakirli Ö., Ibanoğlu C., Güngör C., 2009, New Astron., 14, 496
Çakirli Ö., Ibanoğlu C., Dervisoglu A., 2010, Rev. Mex. Astron. Astrofis., 46, 363
Çakirli Ö., Ibanoğlu C., Sipahi E., 2013, MNRAS, 429, 85
Chabrier G., 2003, ApJ, 586, 133
Chabrier G., Gzllardo J., Baraffe I., 2007, A&A, 472, 17
Chaubey U. S., 1980, Inf. Bull. Var. Stars, 1739, 1
Claret A., 2000, A&A, 359, 289
Coughlin J. L., Shaw J. S., 2007, J. Southeastern Assoc. Res. Astron., 1, 7
Coughlin J. L., López-Morales M., Harrison T. E., Ule N., Hoffman D. I., 2011, AJ, 141, 78
Cox A. N., 2000, Allen's Astrophysical Quantities, 4th edn. Springer, New York, p. 388
Dal H. A., Sipahi E., Özdarcan O., 2012, Publ. Astron. Soc. Aust., 29, 150
Dimitrov D. P., Kjurkchieva D. P., 2010, MNRAS, 406, 2559
Doyle J. G., Mathioudakis M., 1990, A&A, 227, 130
Doyle J. G., Butler C. J., van den Oord G. H. J., Kiang T., 1990, A&A, 232, 83
Eker Z., 1999, ApJ, 512, 386
Fang X. S., Gu S. H., Cheung S. L., Hui H.-K., Kwok C.-T., Leung K.-C., 2010, Res. Astron. Astrophys., 10, 253
Güdel M., 2002, ARA&A, 40, 217
Gunn A. G., Doyle J. G., 1997, A&A, 318, 60
Hall D. S., 1989, Space Sci. Rev., 50, 219
Hall J. C., 2008, Living Rev. Solar Phys., 5, 2
Harrison T. E., Coughlin J. L., Ule N. M., López-Morales M., 2012, AJ, 143, 4
Helminiak K. G., Konacki M., Zloczewski K., 2011, A&A, 527, 14
Helt B. E., 1987, A&A, 172, 155
Henry T. J., Kirkpatrick J. D., Simons D. A., 1994, AJ, 108, 1437
Henry G. W., Eaton J. A., Hamer J., Hall D. S., 1995, ApJS, 97, 513
Holzwarth V., Schüssler M., 2002, Astron. Nachr., 323, 399
Irwin J. et al., 2009, ApJ, 701, 1436
Kamiński K. Z. et al., 2007, AJ, 134, 1206
Kazarovets E. V., Samus N. N., Durlevich O. V., 1998, Inf. Bull. Var. Stars, 4655, 1
Keskin V., Ibanoglu C., Akan M. C., Evren S., Tunca Z., 1994, A&A, 287, 817
Kim S. L., Chun M. Y., Lee W. B., Doyle L., 1997, Inf. Bull. Var. Stars, 4462, 1
Kozhevnikova A. V., Kozhevnikov V. P., Zakharova P. E., Polushina T. S., Svechnikov M. A., 2004, Astron. Rep., 48, 751
Kurucz R. L., 1993, in Milone E. F., ed., Light Curve Modelling of Eclipsing Binary Stars. Springer-Verlag, New York, p. 93
Kwee K. K., van Woerden H., 1956, Bull. Astron. Inst. Neth., 12, 327
Lacy C. H., 1977, ApJ, 218, 444
Lanza A. F., 2010, in Andrei A., Kosovichev A., Rozelot J.-P., eds, Proc. IAU Symp, Vol. 264, Solar and Stellar Variavility: Impact on Earth and Planets. Kluwer, Dordrecht, p. 120
Lanza A. F., Rodonò M., Rosnor R., 1998a, MNRAS, 296, 893
Lanza A. F., Catalano G., Cutispoto G., Pagano I., Rodono M., 1998b, A&A, 332, 541
Lanza A. F., Rodonò M., Mazzola L., Messina S., 2001, A&A, 376, 1011
Lanza A. F., Catalano G., Rodonò M., 2002, A&A, 386, 583
Lee J. W., Youn J. H., Kim S. L., Lee C.-U., 2013, AJ, 145, 16
Li L. F., Zhang F. H., 2006, New Astron., 11, 588
López-Morales M., 2007, ApJ, 660, 732
López-Morales M., Ribas I., 2005, ApJ, 631, 1120
Metcalfe T. S., Mathieu R. D., Latham D. W., Torres G., 1996, ApJ, 456, 356
Moffett T. J., Bopp B. W., 1971, ApJ, 168, 117
Montes D., Fernández-Figueroa M. J., De Castro E., Cornide M., 1995, A&A, 294, 165
Montes D., Fernández-Figueroa M. J., De Castro E., Sanz-Forcada J., 1997, A&AS, 125, 263
Montes D., Crespo-chaón I., Gálvez M. C., Fernández-Figueroa M. J., López-Santiago J., de Castro E., Cornide M., Hernán-Obispo M., 2004, Lecture Notes and Essays in Astrophysics, Vol. 1, Cool Stars: Chromospheric Activity, Rotation, Kinematic and Age. p. 119
Morales J. C., Ribas I., Jordi C., 2008, A&A, 478, 507
Morales J. C., Torres G., Marschall L., Brehm W., 2009, ApJ, 707, 671
Morales J. C., Gallardo J., Ribas I., Jordi C., Baraffe I., Chabrier G., 2010, ApJ, 718, 502
Moss D., 2004, MNRAS, 352, 17
Nefs S. V. et al., 2012, MNRAS, 425, 950
Nelson R. H., 2007, Software by Bob Nelson, available at: http://members.shaw.co/bob.nelson/software1.htm
Nelson T. E., Caton D. B., 2007, Inf. Bull. Var. Stars, 5789
Norton A. J. et al., 2007, A&A, 467, 785
O'Dononghue D., Koen C., Kilkenn D., Stobie R. S., Koester D., Bessell M. S., Hambly N., MacGillivray H., 2003, MNRAS, 345, 506
Olah K., Panov K. P., Pettersen B. R., Valtaoja E., Valtaoja L., 1989, A&A, 218, 192
Orosz J. A., Hauschildt P. H., 2000, A&A, 364, 265
Paschke A., Brát L., 2006, Open Eur. J. Var. Star, 23, 13
Pi Q. F., Zhang L. Y., Li Z. M., Zhang X.-L., 2014, AJ, 147, 50
Pojmański G., 1998, Acta Astron., 48, 35
Pollacco D. L. et al., 2006, PASP, 118, 1407
Pribulla T., Chochol D., Milano L., Errico L., Vittone A. A., Barone F., Parimucha Š., 2000, A&A, 362, 169
Pribulla T., Chochol D., Vittone A. A., 2003, Chin. J. Astron. Astrophys., 3, 361
Pribulla T. et al., 2012, Astron. Nachr., 333, 754
Qian S. B., 2002, PASP, 114, 650
Qian S. B. et al., 2012, MNRAS, 423, 3646
Reid I. N. et al., 2004, AJ, 128, 463
Ribas I., 2006a, Ap&SS, 304, 89
Ribas I., 2006b, in Sterken C., Aerts C., eds, ASP Conf. Ser. Vol. 349, Astrophysics of Variable Stars. Astron. Soc. Pac., San Francisco, p. 55

Ribas I., 2007, in Hartkopf W. I., Guinan E. F., Harmanec P., eds, Proc. IAU Symp, 240, Binary Stars as Critical Tools & Tests in Contemporary Astrophysics. Cambridge Univ. Press, Cambridge, p. 69
Ribas I., Morales J. C., Jordi C., Baraffe I., Chabrier G., Gallardo J., 2008, Mem. Soc. Astron. Ital., 79, 562
Rodonò M., Lanza A. F., Catalano S., 1995, A&A, 301, 75
Rodonò M., Messina S., Lanza A. F., Cutispoto G., Teriaca L., 2000, A&A, 358, 624
Rucinski S. M., 1969, Acta Astron., 19, 245
Rudiger G., Elstner D., Ossendrijver M., 2003, A&A, 406, 15
Scaltriti F., Busso M., Ferrari-Toniolo M., Origlia L., Persi P., Robberto M., Silvestro G., 1993, MNRAS, 264, 5
Skrutskie M. F. et al., 1997, in Garzon F. et al., eds, Astrophysics and Space Science Library, Vol. 210, The Impact of Large Scale Near-IR Sky Surveys. Kluwer, Dordrecht, p. 25
Strassmeier D., 2009, A&AR, 17, 251
Tokunaga A. T., 2000, in Cox A. N., ed., Allen's Astrophysical Quantities, 4th edn. Springer, New York, p. 143
Torres G., Ribas I., 2002, ApJ, 567, 1140
Van Hamme W., 1993, AJ, 106, 209
Vida K., Olah K., Kovari Zs., Korhonen H., Bartus J., Hurta Zs., Poszto-báányi K., 2009, A&A, 504, 1021
Wilson R. E., 1990, ApJ, 356, 613
Wilson R. E., 1994, PASP, 106, 921
Wilson R. E., Devinney E. J., 1971, ApJ, 166, 605
Wilson R. E., Van Hamme W., 2004/2010, Computing Binary Star Observables. Univ. Florida, Gainesville, FL
Windmiller G., Orosz J. A., Etzerl P. B., 2010, ApJ, 712, 1003
Wolf M., Zejda M., Mikulascaron J., Janík J., Chrastina M., Skarka M., Dróóżdż M., Kreiner J., 2010, in Prša A., Zejda M., eds, ASP Conf. Ser. Vol. 435, Binaries - Key to Comprehension of the Universe. Astron. Soc. Pac., San Francisco, p. 441
Woźniak P. R. et al., 2004, AJ, 127, 2436
Zeilik M., De Blasi C., Rhodes M., Budding E., 1988, ApJ, 332, 293
Zeilik M., Cox D. A., De Blasi C., Rhodes M., Budding E., 1989, ApJ, 345, 991
Zeilik M., Gordon S., Jaderlund E., Ledlow M., Summers D. L., Heckert P. A., Budding E., Banks T. S., 1994, ApJ, 421, 303
Zhang L. Y., 2010, PASP, 122, 309
Zhang L. Y., 2011, in Qain S., Leung K., Zhu L., Kwok S., eds, ASP Conf. Ser. Vol. 451, 9th Pacific Rim Conference on Stellar Astrophysics. Astron. Soc. Pac., San Francisco, p. 123
Zhang L. Y., 2012, Res. Astron. Astrophys., 12, 433
Zhang L. Y., Gu S. H., 2007, A&A, 471, 219
Zhang L. Y., Gu S. H., 2008, A&A, 487, 709
Zhang X. B., Zhang R. X., 2007, MNRAS, 382, 1133
Zhang L. Y., Zhang X. L., Zhu Z. Z., 2010a, New Astron., 15, 362
Zhang L. Y., Jing, J H., Tang Y. K., Zhang X. L., 2010b, New Astron., 15, 653
Zhou A. Y., Jiang X. J., Zhang Y. P., Wei J.-Y., 2009, Res. Astron. Astrophys., 9, 349

SUPPORTING INFORMATION

Additional Supporting Information may be found in the online version of this article:

Table 3. *VRI* observations data of the five low-mass eclipsing binaries collected 2010–2012.
Table 5. All compiled light minimum times of the low-mass eclipsing binaries.
Figure 6. The configurations of the five low-mass eclipsing binaries.
Figure 7. All the collected published LCs and their corresponding theoretical LCs based on our new orbital parameters (http://mnras.oxfordjournals.org/lookup/suppl/doi:10.1093/mnras/stu964/-/DC1).

Please note: Oxford University Press is not responsible for the content or functionality of any supporting materials supplied by the authors. Any queries (other than missing material) should be directed to the corresponding author for the paper.

This paper has been typeset from a TEX/LATEX file prepared by the author.